

Prospects of detecting the reactor $\bar{\nu}_e$ -Ar coherent elastic scattering with a low threshold dual-phase argon time projection chamber at Taishan

Yu-Ting Wei^{1,2}, Meng-Yun Guan¹, Jin-Chang Liu^{*1}, Ze-Yuan Yu^{†1}, Chang-Gen Yang^{1,2}, Cong Guo¹, Wei-Xing Xiong^{1,2}, You-Yu Gan^{1,2}, Qin Zhao^{1,2}, and Jia-Jun Li^{1,3}

¹*Institute of High Energy Physics, CAS, Beijing 100049, China*

²*University of Chinese Academy of Sciences, Beijing 100049, China*

³*North China Electric Power University, Beijing 100096, China*

March 22, 2021

Abstract

We propose to measure the coherent elastic neutrino-nucleus scattering (CE ν NS) using a dual-phase liquid argon time projection chamber (TPC) with 200 kg fiducial mass. The detector is expected to be adjacent to the JUNO-TAO experiment and to be about 35 m from a reactor core with 4.6 GW thermal power at Taishan. The antineutrino flux is approximately $6 \times 10^{12} \text{ cm}^{-2} \text{ s}^{-1}$ at this location, leading to more than 11,000 coherent scattering events per day in the fiducial mass. However, the nuclear recoil energies concentrate in the sub-keV region, corresponding to less than ten ionization electrons in the liquid argon. The detection of several ionization electrons can be achieved in the dual-phase TPC due to the large amplification in the gas region. With a feasible detection threshold of four ionization electrons, the signal rate is 955 per day. The detector is designed to be shielded well from cosmogenic backgrounds and ambient radioactivities to reach a 16% background-to-signal ratio in the energy region of interest. With the large CE ν NS sample, the expected sensitivity of measuring the weak mixing angle $\sin^2 \theta_W$, and of limiting the neutrino magnetic moment are discussed. In addition, a synergy between the reactor antineutrino CE ν NS experiment and the dark matter experiment is foreseen.

keywords: coherent elastic neutrino-nucleus scattering, dual-phase argon TPC, reactor antineutrinos

1 Introduction

There has been over forty years since D. Freedman predicted the coherent elastic neutrino-nucleus scattering process (CE ν NS) [1]. In the weak neutral current, the $\nu + A \rightarrow \nu + A$ elastic scattering process should have a sharp coherent forward peak for $qR \ll 1$. Here, q is the absolute momentum transfer from the neutrino to the nucleus, and R is the weak nuclear radius. The CE ν NS is dominated interaction for neutrinos with energies less than ~ 100 MeV. It has been firstly observed at a 6.7σ confidence level with a CsI[Na] detector in the COHERENT experiment [2]. It used pulsed neutrinos from the Spallation Neutrino Source (SNS). Later on, the ν -Ar coherent scattering is also detected by the COHERENT experiment using a single phase liquid argon detector [3]. Since the neutrinos are produced in the pion-decay-at-rest process, the nuclei recoil energy concentrates in a range of several to tens of keV (keV_{nr}).

Given the high cross section and the unique properties of the CE ν NS process, many studies have been carried out using the COHERENT data. For example, the weak mixing angle is measured at the low momentum transfer [4]. The average CsI neutron density distribution is obtained [5]. When endowed with mass and electromagnetic properties, the neutrino magnetic moment μ_ν [6] and the neutrino charge radius [7] are limited. On the other hand, via the CE ν NS process, astrophysical neutrinos create an unavoidable background in the

*liujinc@ihep.ac.cn

†yuzy@ihep.ac.cn

experiments searching for the WIMP dark matter [8–10], that is the ‘neutrino floor’. In addition, the search for low-mass WIMP using the ionization signal only has drawn more and more attention [11–13]. Understanding the response of LXe and LAr from sub-keV to several keV nuclear recoil energies is crucial to the search for light dark matter via this approach.

Given such abundant physics topics, many experiments are on projecting or proceeding [14]. Larger detectors with lower detection threshold will be employed in the COHERENT experiment [15]. On the other hand, experiments using the strongest artificial neutrino source on the Earth, i.e., the nuclear reactors, are growing quickly, such as CONNIE [16], MINER [17], CONUS [18], and Red-100 [19]. Compared to the neutrinos with energies of a few tens MeV at SNS, the 2 MeV average energy of reactor antineutrinos requires a significant reduction of the detection threshold. Thus, the corresponding detectors used in the above experiments are the cryogenic Ge/Si detector, or the dual-phase Xe Time Projection Chamber (TPC).

In this paper, we propose an experiment to measure the coherent scattering between reactor $\bar{\nu}_e$ ’s and argon nuclei using a dual-phase argon TPC at Taishan, referred to as Taishan Coherent Scattering Experiment here after. The Taishan Coherent Scattering Experiment will use 200 kg argon as target and will be located side-by-side with the JUNO-TAO experiment [20], which aims to precisely measure the reactor $\bar{\nu}_e$ spectrum using a ton-scale liquid scintillator detector with a percent level energy resolution. The antineutrino flux is approximately $6 \times 10^{12} \text{ cm}^{-2} \text{ s}^{-1}$ at this location, and the vertical overburden is about 5 meters of water equivalent (m.w.e.) [20]. The TPC size is limited primarily by the size of the elevator to enter the lab. Thus, the maximum fiducial argon mass is 200 kg.

There are many advantages of using argon in the detection of CE ν NS. As a noble element detector, the target mass is easy to reach hundreds of kilograms. This leads to much larger statistics compared to the kg-scale Ge/Si detectors. Although the ν –Xe CE ν NS cross section is about 16 times larger than that of ν –Ar, due to the mass of an argon nucleus is approximately 3.4 times smaller than xenon, the larger nuclear recoil energy leads to much easier detection in argon. The large CE ν NS sample not only allows to measure the weak mixing angle $\sin \theta_W$ using the reaction rate, but also opens a door to explore more physics using the spectral shape, for example, constraining the neutrino magnetic momentum, and measuring the ionization electron yield at keV_{nr} energy range. The major problem of using argon is the intrinsic 1 Bq/kg ^{39}Ar decays in the atmospheric argon (AAr). A possible solution is to use the depleted underground argon (UAr) [21]. As a feasibility study, we will use a 0.7 mBq/kg ^{39}Ar decay rate in the following sections.

The paper is structured as follows: Sec. 2 presents the conceptual design of the low threshold Argon TPC detector. Sec. 3 focuses on the background simulation and the design of shielding. Sec. 4 presents the study of expected sensitivities. A short summary and prospects are discussed in Sec. 5.

2 Conceptual design of Taishan Coherent Scattering Experiment

In the Standard Model, the differential cross section of CE ν NS is expressed as:

$$\frac{d\sigma}{dT_N}(E_\nu, T_N) \simeq \frac{G_F^2}{4\pi} M Q_W^2 \times \left(1 - \frac{MT_N}{2E_\nu^2}\right) F_W^2(q^2), \quad (1)$$

where E_ν is the energy of the neutrino, G_F is the Fermi constant, M is the nucleus mass, and T_N is the nuclear recoil energy. The weak charge Q_W is defined as:

$$Q_W = N - (1 - 4 \times \sin \theta_W) \cdot Z, \quad (2)$$

where N and Z are the numbers of neutrons and protons in the nucleus, and θ_W is the Weinberg mixing angle. The weak form factor $F_W^2(q^2)$ is taken as 1 due to the low q values in the scattering between reactor $\bar{\nu}_e$ ’s and nuclei [22].

Using the reactor neutrino spectra in the 2-8 MeV range provided in Refs. [23, 24] and applying an exponential extrapolation for spectra below 2 MeV, the nuclear recoil energy spectra of Ar are calculated and shown in Fig. 1. The $\bar{\nu}_e$ -Ar CE ν NS reactions from neutrinos in sliced energy ranges (0-1 MeV; 1-1.8 MeV; 1.8-3 MeV; 3-10 MeV) are also drawn for better illustration. The detection of reactor $\bar{\nu}_e$ ’s with energies smaller than 1.8 MeV, i.e., below the threshold of the inverse-beta-decay reaction, is quite difficult. Because the nuclear

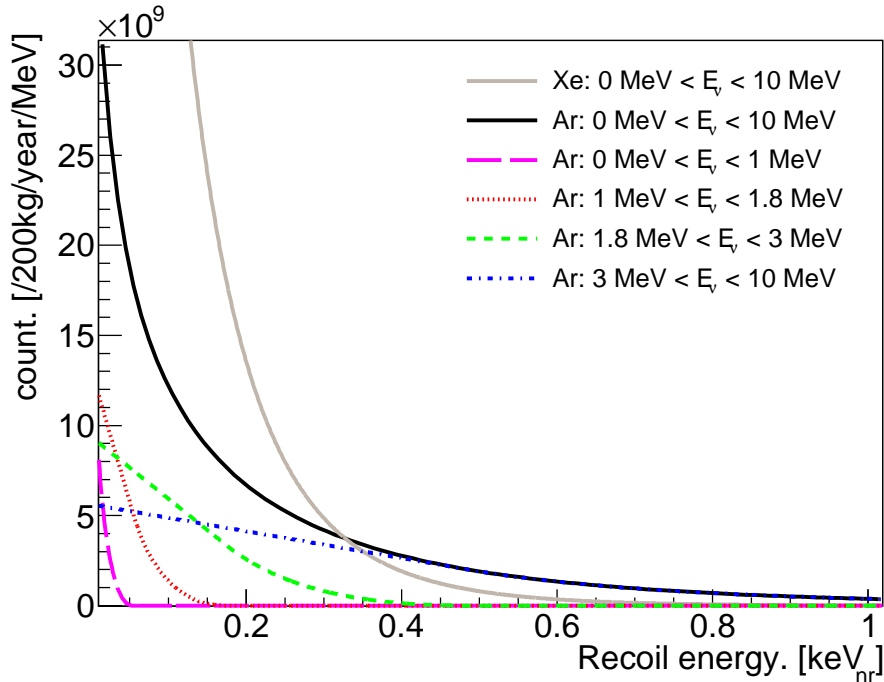


Figure 1: Recoil energy spectra of Ar and Xe nuclei in the reactor $\bar{\nu}_e$ CE ν NS reaction.

recoil energy is less than $0.15 \text{ keV}_{\text{nr}}$ where the electron yield is about $6.4 \text{ e}^-/\text{keV}_{\text{nr}}$, corresponding to a single ionization electron. In the energy region above $0.2 \text{ keV}_{\text{nr}}$, the signals are dominated by $\bar{\nu}_e$'s with energies larger than 3 MeV . This puts a stringent requirement on lowering the detection threshold to sub- keV_{nr} .

The dual-phase TPC using argon or xenon suits such low energy detection. An obvious advantage of argon is the smaller nucleus mass than xenon. The signal rate on argon is larger than that on xenon with the same target mass when the recoil energy is larger than $0.17 \text{ keV}_{\text{nr}}$. To estimate a feasible detection threshold, we take the experience from the DarkSide-50 and the Red-100 experiments. The DarkSide-50 dual-phase argon TPC has achieved the detection of single ionization electron and the analysis of energy threshold above 4 ionization electrons. The latter value corresponds to approximately $0.5 \text{ keV}_{\text{nr}}$ [11]. The Red-100 experiment has performed the first ground-level laboratory test of the dual-phase xenon TPC and proved the feasibility of a threshold of 4 ionization electrons (about $0.6 \text{ keV}_{\text{nr}}$ in xenon) [19, 25, 26]. Thus, we will use 4 ionization electrons (about $0.5 \text{ keV}_{\text{nr}}$ in argon) as the analysis threshold in the following studies.

The proposed Taishan Coherent Scattering Experiment will be located side-by-side with the JUNO-TAO experiment in the Taishan Nuclear Power Plant. There are two reactor cores in operation now. Each of them has a thermal power of 4.6 GW . The experiment will be in a basement of an elevation of -9.6 meters , in which the measured cosmic-ray muon flux is one third of that at the ground level. The argon TPC is approximately 35 m to one reactor core and is 253 m to another one. The entrance to the laboratory relies on an elevator with a width of 1.39 m and a height of 1.99 m . Thus, the size of TPC together with the outer shielding and insulation materials is limited to 1.4 m and the total fiducial mass is about 200 kg . In addition, the height of the detector, including the shield, should be less than 3.85 m due to the limitation of experimental hall space.

Figure 2 shows the conceptual design of the dual-phase argon TPC detector. The most inner region is the sensitive argon target (SensAr). A cylindrical acrylic vessel (57 cm height, 57 cm diameter) is used to hold $\sim 200 \text{ kg}$ liquid argon. A drift electric field is applied in the vertical direction by the high voltage on the copper rings. A gas argon layer with a height of 1.5 cm is above the liquid argon. A luminescent electric field is applied in the gas region for the single ionization electron detection. The energy deposition in liquid argon produces photons and free electrons. The photons are promptly detected by photosensors and are commonly named as S1. The free electrons will drift to the gas layer in the vertical electric field. Then, one electron could generate an electroluminescence signal named as S2. The S2 photoelectron (p.e.) yield can reach $23 \pm 1 \text{ p.e./e}^-$ [11]. The

time between S1 and S2 is the drift time corresponds to the time it takes for electrons to move from the action point to the gas phase. The electron drift speed is related to the strength of the drift electric field [27]. In the reactor $\bar{\nu}_e$ -Ar CE ν NS reaction, it is great difficulty to detect S1. For the argon detector, the better light yield is about 10 PE/keV $_{ee}$ for S1. So the S1 is few and even zero PE in the sub-keV $_{nr}$ considering the quenching factor. Thus, the experiment would rely on S2 only. A set of photosensor array is equipped on the top and the bottom of the TPC. The photon sensitive coverage is 30% similar to that of DarkSide-50. To simulate the background, 44*2 Hamamatsu R-11065 PMTs are used as the photon sensor array.

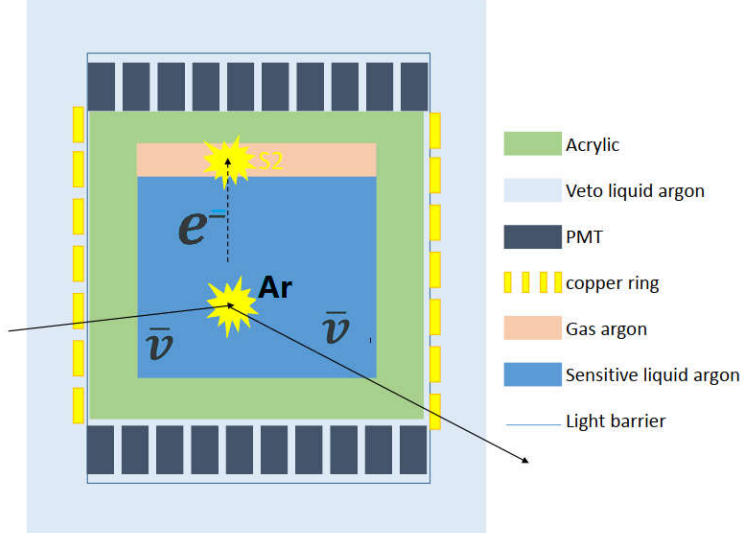


Figure 2: Conceptual design of the dual-phase argon TPC at Taishan. The veto liquid argon detector is of great importance to tag the multiple scattering γ 's and neutrons.

3 Veto and shielding design

Although the number of CE ν NS signals could reach 1,000 per day in the 200 kg argon target above a detection threshold of 4 ionization electrons, the signals could be easily washed out by the backgrounds from cosmic ray muons (about 60 Hz/m²) and ambient radioactivity decays. To design the veto and shielding, lots of simulation are carried out using Geant4 [28]. The ambient radioactivity and cosmic ray muons are simulated. The concentrations of ²³⁸U, ²³²Th, and ⁴⁰K in the materials are listed in Table 1. The muon generators are taken from the JUNO-TAO simulation [20]. The veto and shielding design is shown in Fig. 3.

material	weight	Data source	²³⁸ U mBq/kg	²³² Th mBq/kg	⁴⁰ K mBq/kg
Lead	101 t	radiopurity.org	60	-	14
PP	32 t	radiopurity.org	9.84	0.569	<3.1
Acrylic	(814+190) kg	JUNO-TAO	<0.0123	<4.07 × 10 ⁻³	<3.1 × 10 ⁻⁵
Copper ring	40 kg	DarkSide-50	<0.06	<0.02	0.12
3" PMT R11065	44 × 2	Darkside-50	5.2 mBq/PMT	13.4 mBq/PMT	37.1 mBq/PMT
concrete	400 t	JUNO-TAO	5.8 × 10 ⁴	7.9 × 10 ⁴	7.8 × 10 ⁵

Table 1: Concentrations of radioactive impurities of materials.

The outermost layer is plastic scintillator with 5 cm thickness to tag cosmic ray muons. The inner brown

layer stands for 15 cm lead to shield the ambient radioactivity from hall. Then, a polypropylene layer acts as thermal insulation and also can shield neutrons generated by muons. With 90 cm polypropylene, the acrylic vessel can keep $-186\text{ }^{\circ}\text{C}$ stably.

There are two liquid argon detectors, the outer liquid argon detector is served as a veto detector, instrumented with photosensors and named as the VetoAr, and the inner detector is the aforementioned dual-phase liquid argon TPC, used to detect $\bar{\nu}_e$'s and named as the SensAr. The VetoAr not only passively shields the SensAr from radioactivity from outer materials or hall concrete, but also can tag the multiple scattering γ s or neutrons. Once the VetoAr observes an energy deposit, a $600\text{ }\mu\text{s}$ veto window could be applied to the SensAr according to the maximum drift time of electrons from the TPC bottom to the top. Since most of backgrounds are from gammas, a quenching factor of 0.25 [29] is used to convert the nuclear recoil energy and the electron energy, that is, $1\text{ keV}_{\text{ee}} = 4\text{ keV}_{\text{nr}}$. In the following sections, the backgrounds are provided in the energy range of 0 to 1 keV_{ee} , corresponding to 0 to 4 keV_{nr} .

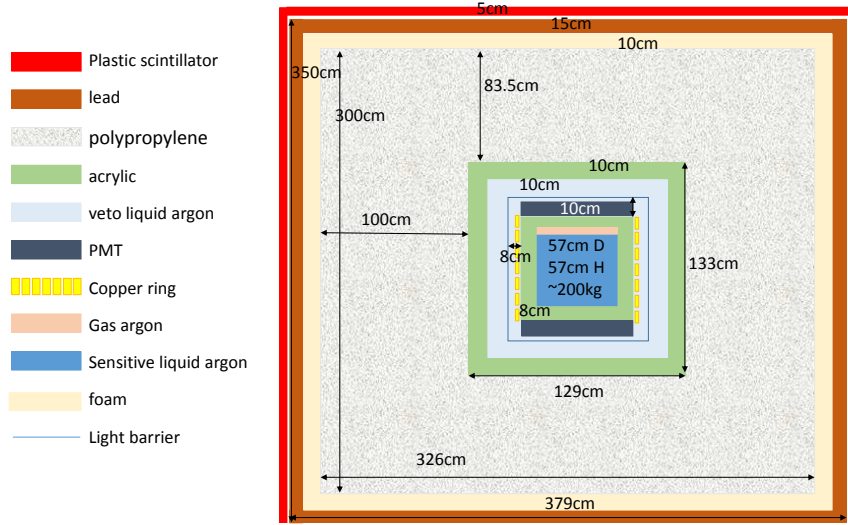


Figure 3: Conceptual design of veto and shielding of the Taishan Coherent Scattering Experiment.

3.1 Natural radioactivity

3.1.1 Backgrounds from the hall

In the simulation of the natural radioactive decays in the concrete of the hall, the simulation generators including the $\gamma/\alpha/e^-$ from radioactive decay are placed in the shell extending 30 cm into the inner wall. According to simulation results, the gamma rays beyond the 30 cm are almost impossible to transport into the sensitive argon. Figure 4 shows the energy spectrum in the SensAr after shielded by 15 cm lead and other inner materials. The background level is about $0.22\text{ /day/kg/keV}_{\text{ee}}$ in the 0 to 1 keV_{ee} energy region. Considering the 101 t weight of the 15 cm lead, different thicknesses of lead are also simulated, listed in Table 2. It can be found that the 15 cm lead is difficult to reduce.

In addition to the gammas, fast neutrons could be produced via the (α, n) reaction and in the ^{238}U spontaneous fission, named as radiogenic neutrons. The neutron flux from Hall is estimated as $2.0 \times 10^{-6}\text{ /cm}^2/\text{s}$ [30], and the average neutron kinetic energy is about 1.7 MeV. The attenuation length of neutron is about 6.8 cm in the material that contains 10% hydrogen. After about 90 cm polypropylene, the neutron flux could be reduced by 10^6 . Thus, the radiogenic neutron contributes only a few background per day

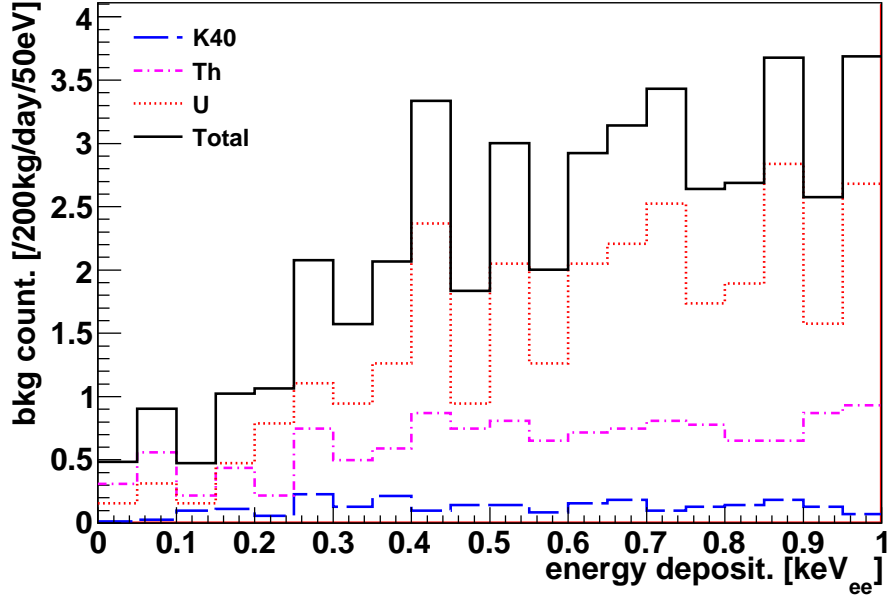


Figure 4: The deposit energy spectrum in the SensAr from natural radioactivity decays in the hall concrete after shielded by 15 cm lead and other detector materials.

Lead Thickness.	15 cm	13 cm	10 cm
Background	0.22	0.91	5.37

Table 2: Background level (/day/kg/keV_{ee}) in the SensAr from the hall concrete after shielded by different thickness of lead.

that can be ignored.

3.1.2 Backgrounds from the detector material

The background contributions in the SensAr from major detector components are listed in Table 3. If the energy deposit in the VetoAr is larger than 0.1 MeV, this event triggers the veto argon detector, and a subsequent 600 μ s veto window is applied in the sensitive detector. Here list the statistics of radioactivity counts ($E_{\text{dep}} > 0.1$ keV) and also list the count of the energy interval ($0.1 \text{ keV} < E_{\text{dep}} < 1 \text{ keV}$). The radioactivity from material could be vetoed by veto argon detector. The threshold in the veto detector is also varied, and the corresponding veto efficiency is shown in Fig. 5. The different color mean different material. For higher veto efficiency and lower trigger, an energy threshold of 0.1 MeV is recommended. The "E_{dep}" is the energy deposit in the sensitive argon. The total trigger rate will be about 2 Hz in the sensitive detector. With the help of the VetoAr, the background in the energy range of interest is only 18 per day in SensAr, much smaller than the 1,000 signals.

Material		Lead	PP	OutAcrylic	InnerAcrylic	Cage	PMTs	Total
$E_{\text{dep}} > 0.1 \text{ keV}$	No veto	34753	60060	40	251	28580	50596	174280
$0.1 \text{ keV} < E_{\text{dep}} < 1 \text{ keV}$		11.2	25.9	0	0.14	10.4	26.5	74.2
$E_{\text{dep}} > 0.1 \text{ keV}$	After veto	14576	19658	5.5	172	13357	14990	62758
$0.1 \text{ keV} < E_{\text{dep}} < 1 \text{ keV}$		4.1	4.7	0	0.1	3.3	5.6	17.8
Dead time		1.1%	1.4%	0.0%	0.25%	0.1%	0.2%	3.0%

Table 3: Background rates in the SensAr per 200 kg per day. The veto means a larger than 0.1 MeV energy deposit is found in the VetoAr, then, a subsequent 600 μ s veto is applied in the SensAr.

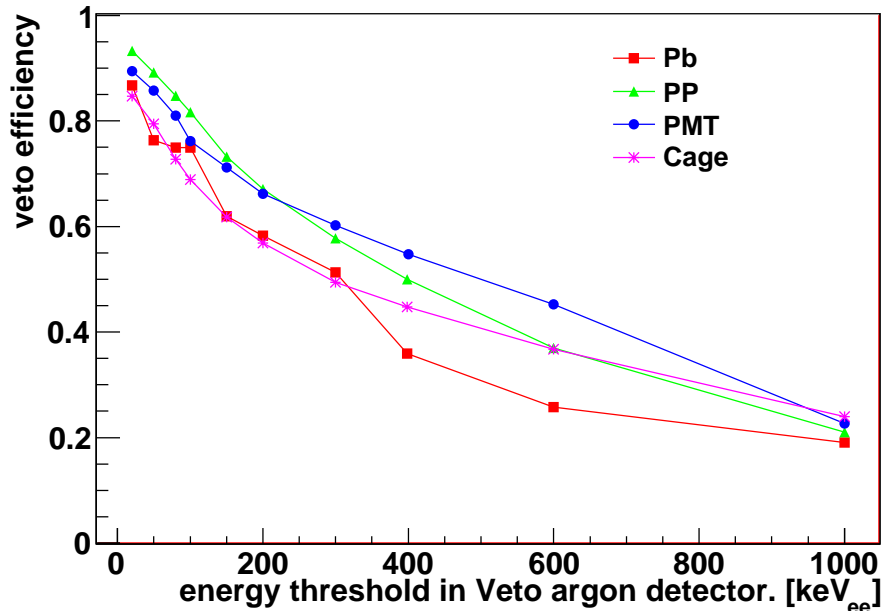


Figure 5: Veto efficiency with respect to the energy threshold in the veto argon detector

Another crucial background comes from the intrinsic ^{39}Ar and ^{85}Kr decays in the argon. It is well known that the ^{39}Ar concentrations in the argon from atmosphere (AAr) or underground (UAr) are quite different as shown in Table 4 [21,31]. If the AAr is used in the SensAr, the number of ^{39}Ar decays in the energy of interest could reach 40 times of the signal. Thus, UAr is a must for the detection of CE ν NS using reactor $\bar{\nu}_e$'s. In this case, the background rate is 25 per day per 200 kg in the energy range of interest. If the AAr is used in VetoAr, the dead time could reach more than 50%.

^{39}Ar in underground Ar	0.73 ± 0.11 mBq/kg
^{39}Ar in atmospheric Ar	$(1.01 \pm 0.08) \times 10^3$ mBq/kg
^{85}Kr in Ar	2.05 ± 0.13 mBq/kg

Table 4: Intrinsic radioactivity in liquid argon. The data are taken from Refs. [21,31].

As a short summary, the energy spectra of backgrounds from materials are shown in Fig. 6. The residual backgrounds are dominated by the intrinsic ^{39}Ar and ^{85}Kr decays. A lower ^{85}Kr concentrations could be achieved using the distillation at low temperature.

3.2 Cosmic ray muons

Although most of the hadronic components of cosmic rays have been absorbed, the muons with a rate of ~ 60 Hz/m² in the experimental hall would contribute significant backgrounds if they are not well tagged. In the conceptual design, two detectors are employed to tag the muons. The first one is a layer of plastic scintillator with 5 cm thickness as the outmost tag. The VetoAr detector is used to tag muons close to the sensitive argon TPC as Fig. 3. Table 5 summarizes the rates and veto efficiency of muons and secondary particles in different detectors. Figure 7 shows the time interval distribution between the energy deposit in SensAr and the corresponding muon. Black line shows the all events in SensAr; blue line shows the residual events after the veto of plastic scintillator; red line shows the residual events after the vetof of VetoAr. For illustration, the time interval longer than 30 μs is filled in the bin of 29 μs . There are two typical cases to discuss.

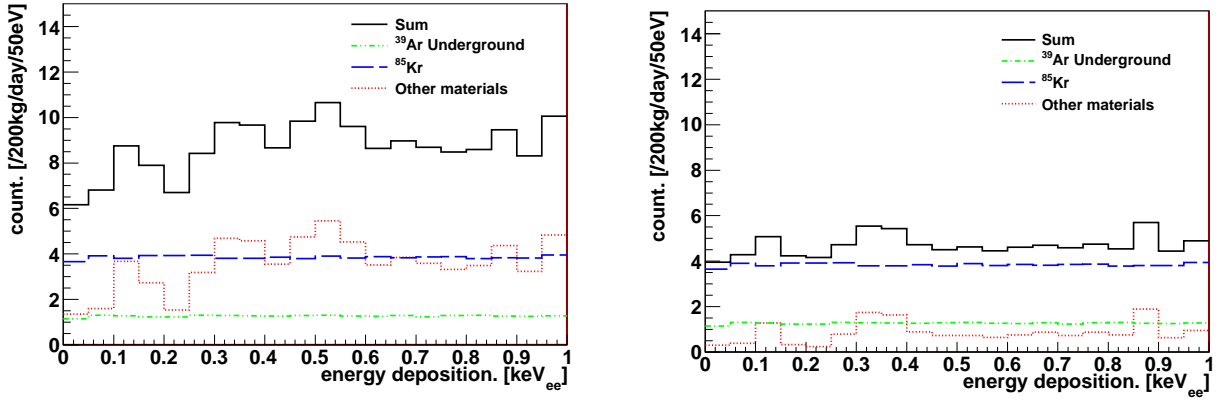


Figure 6: Backgrounds from materials before (left) and after (right) implementing the veto of VetoAr.

Detector	Plastic scintillator	Veto argon	Sensitive argon
Rate. Hz	3421	325	106
veto efficiency. %	95.7%	97.8%	-

Table 5: Rates and veto efficiency of cosmic ray muons and their secondary particles in different detectors.

I. Muons passing through or stopped in the SensAr or VetoAr. Once a large energy deposit is found in the two detectors, a subsequent $600 \mu s$ veto window is applied in the SensAr. Neutrons or radioactive nuclei could be produced in the interaction of cosmic ray muon and detector materials, such as radioisotopes of S/Cl/Ar/K. The energetic particles generated in the neutron capture and the nuclei decays form the long tail in the time interval distribution. The $600 \mu s$ veto window removes most of neutrons and muon decay signals. The events with longer life are difficult to be vetoed. The VetoAr could reduce significantly such background because a γ from the decay of cosmogenic isotopes could deposit energy both in the VetoAr and SensAr detectors, shown as the red line in Fig. 7.

II. For muons only passing through the plastic scintillator detector, the plastic scintillator could tag them with a very high efficiency. Due to the 3400 Hz trigger rate of the plastic scintillator detector, the subsequent correlation time window with the argon detectors could set only to 1 to $10 \mu s$. It could help to classify the events in the argon detectors, as cosmic ray muons contribute the largest trigger rate in the argon detectors, as listed in Table 6.

3.3 Summary of background rates and the detector live time

Table 6 lists the summary of background rates and dead time. The veto time window is $600 \mu s$ in SensAr once the VetoAr observes an energy deposit larger than 0.1 MeV. This design significantly reduces the background in the SensAr. A $10 \mu s$ correlation window will be used between the argon detectors and the plastic scintillator

	Concrete of Hall	Material	Muon	Total
Rate in SensAr ($> 0.1 \text{ keV}_{ee}$)	1.1 Hz	2.6 Hz	106 Hz	109.7 Hz
Rate in VetoAr ($> 0.1 \text{ MeV}_{ee}$)	-	53 Hz+(711 Hz)	325 Hz	378 Hz+(711 Hz)
Dead time	-	3.2% + (42%)	19.5%	22.5% + (42.0%)
Bkg after veto in $0.1\text{-}1 \text{ keV}_{ee}$ /keV/kg/day	0.22	$0.09 + 0.12 + 0.38$ Materials+ ^{39}Ar + ^{85}Kr	0.61	1.42

Table 6: Summary of background rates, and the veto dead time. The numbers in the brackets stands for the case that the air argon is used in the veto argon detector.

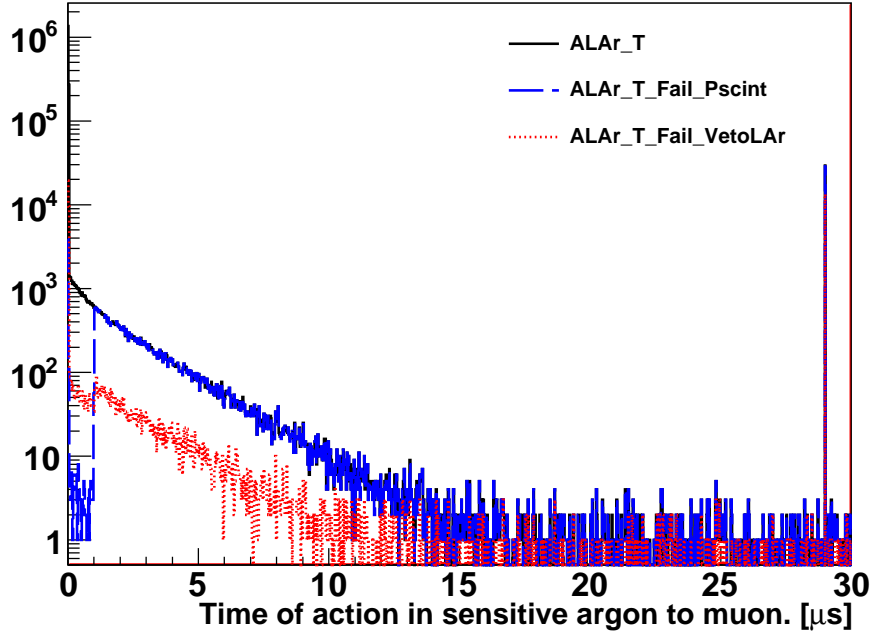


Figure 7: Time distribution to last muon of energy deposit in SensAr. Black line shows the all events in SensAr; blue line shows the residual events after the veto of plastic scintillator; red line shows the residual events after the veto of VetoAr.

detector. A crucial requirement is that the argon of SensAr must be low radioactivity underground one. Using UAr in the VetoAr is not necessary, but it can save the 42% dead time as the value in the brackets. Moreover, the low trigger rate in VetoAr by using underground argon can help set up an online anti-coincidence to reduce the amount of data. After shielding and veto, the background level is about 1.424 event/kg/keV/day in 0.1-1 keV_{ee}.

4 Expected sensitivity of the Taishan Coherent Scattering Experiment

With the $\sim 1,000$ CE ν NS signals per day of the Taishan Coherent Scattering Experiment above the 0.5 keV_{nr} threshold, many physics topics can be studied, for example, the weak mixing angle at low momentum transfer and the neutrino magnetic moment, etc. Moreover, the reactor $\bar{\nu}_e$'s, with 2%~3% spectrum shape precision measured in Ref. [32], provide a powerful tool to study the ionization electron yield at keV_{nr} energy range. This will benefit the search of low-mass WIMP dark matter, in particular for the analyses using the ionization signal only [11, 33]. A synergy between the neutrino detector and the dark matter detector is foreseen. Some discussions are presented in this section.

To perform these analyses, a simplified detector response is added to the signal and background spectra. The first step is to convert the nuclear recoil energy and the electron energy to the number of ionization electrons (N_{e^-}). The ionization electron yield (Y_{e^-}) refers to the results in Ref. [11]. As mentioned above, a quenching factor of 0.25 is used between keV_{ee} and keV_{nr}. The N_{e^-} distribution is assumed to follow the Poisson distribution. The electron extraction efficiency is set to 100%. Figure 8 shows the CE ν NS signal and background spectra in the unit of ionization electrons. To get a good signal to background ratio, the energy region of interest is selected to 4 to 11 e^- . The 4 e^- is chosen to get rid of the backgrounds released by impurities after a large energy deposit. In the 4 to 11 e^- energy range, the number of signals and background events is 955 and 153, respectively, per day per 200 kg argon.

In the future, the background can be measured *in-situ* using the reactor on-off information. According to the reactor running status, there would be an one-month reactor off period per year. The background can be

measured to a statistic of $N_{\text{bkg}} = 153/\text{day} \times 30 \text{ days} = 4590$. This corresponds to a statistical uncertainty of $\sigma_{\text{bkg}} = 1/\sqrt{N_{\text{bkg}}/N_{\text{bin}}} = 4.2\%$ per ionization electron bin. This number will be used in the following analyses.

The systematic uncertainties consist of the trigger efficiency, the target mass, and the reactor $\bar{\nu}_e$ rate and spectrum. According to Ref. [11], the trigger efficiency has reached to 100% at 4 ionization electrons. Since all the sensitive argon is held in the acrylic vessel, no fiducial volume cut is used, the target mass uncertainty only arises from the liquid level instability. The $\bar{\nu}_e$ prediction will benefit from the reactor neutrino experiments using the IBD channel [20, 32, 34, 35]. Thus, 1% (aggressive) and 3% (conservative, nominal) bin-to-bin correlated uncertainties will be tested.

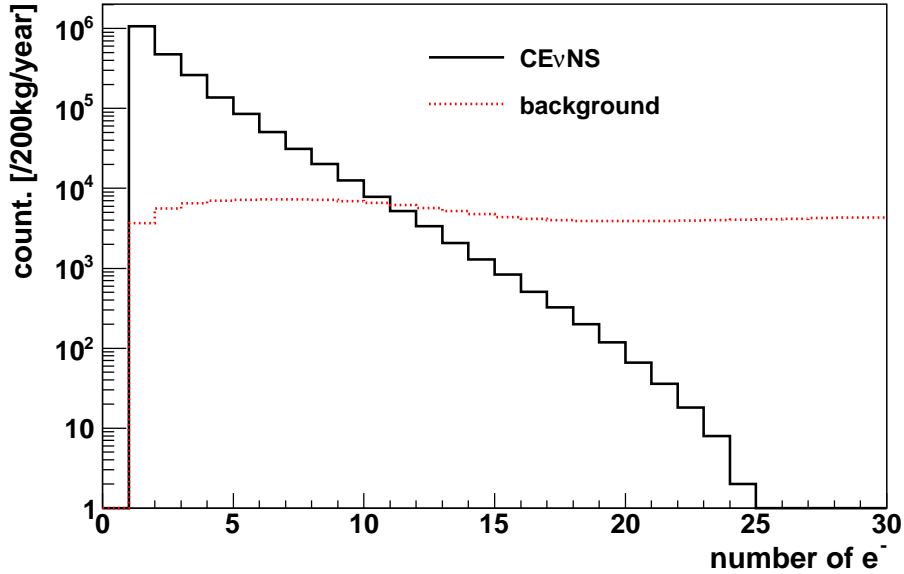


Figure 8: Spectra of $\text{CE}\nu\text{NS}$ signals and simulated background, taken a simplified detector response into consideration.

The measured $\text{CE}\nu\text{NS}$ spectrum in terms of the number of ionization electrons is sensitive to several parameters. Here, we take the weak mixing angle $\sin^2 \theta_W$, the neutrino magnetic moment ν_μ , and the ionization electron yield Y_{e^-} for illustration. The nominal value of $\sin^2 \theta_W$ is set to 0.2386 according to the Particle Data Group [36], ν_μ is set to 0, and Y_{e^-} to 7 per keV_{nr} . Then, three spectra are generated by changing one parameter and keeping the other two unchanged. Their ratios to the nominal spectrum are shown in Fig. 9. The weak mixing angle $\sin^2 \theta_W$ changes the number of events in all the bins by the same ratio. An obvious upward trend is found when Y_{e^-} is enlarged by 10%. It means the Y_{e^-} can be extracted by fitting the measured spectrum shape with the high statistics data. This provides a unique probe to calibrate the ionization electron yield in sub- keV_{nr} energy range, in which there is no suitable neutron source up to now. Finally, if a non-zero ν_μ value is introduced, a downward trend is found, since the $\text{CE}\nu\text{NS}$ cross section will be plus the term:

$$\frac{d\sigma_{\mu\nu}}{dT_N}(E_\nu, T_N) = \frac{\pi\alpha^2}{m_e^2} \left| \frac{\mu_\nu}{\mu_B} \right|^2 \frac{Z^2}{T_N} \left(1 - \frac{T}{E_\nu} + \frac{T^2}{4E_\nu^2} \right). \quad (3)$$

To obtain a expected sensitivity for the parameters, a χ^2 function is defined as:

$$\chi^2 = \min_{\alpha, \beta} \sum_{i=4e^-}^{i=11e^-} \left(\frac{(N_{\text{data}}^i - N_{\text{Fit}}^i (1 + \alpha) - \text{Bkg}^i)^2}{N_{\text{data}}^i + \beta^i \times \text{Bkg}^i} \right) + \left(\frac{\alpha}{\sigma_\alpha} \right)^2, \quad (4)$$

where N_{data}^i is the measured candidates in the i th bin, and N_{data}^i is the predicted number of $\text{CE}\nu\text{NS}$ signals. The exposure is set to 200 kg·year. The Bkg^i is the number of background in the i th bin, and can be estimated

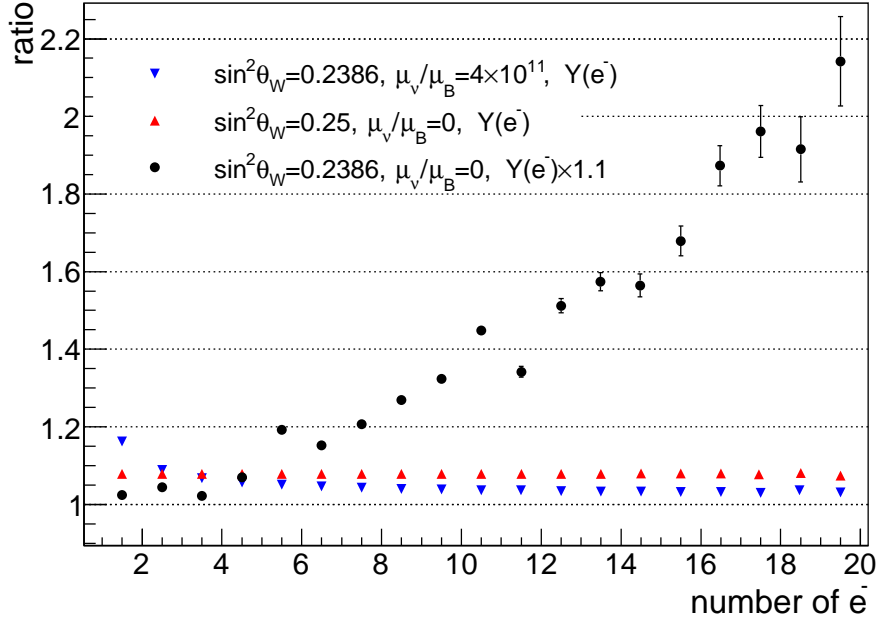


Figure 9: Ratios of spectra with different parameter values to nominal spectrum. Details are found in the text.

using the reactor off data as mentioned above. Thus, the 4.6% background uncertainty is treated as bin-to-bin uncorrelated as β^i in the denominator. The nuisance parameter α stands for the systematic uncertainty, and 3% is used conservatively as the nominal value. The results with 1% systematic uncertainty are also shown in the plots.

By minimizing the χ^2 function, the expected sensitivities of $\sin^2 \theta_W$ and μ_ν are obtained and shown in Fig. 10. The 90% C.L. of $\sin^2 \theta_W$ is 0.232 to 0.246 at keV energy transfer. The upper limit of the neutrino magnetic moment is $\mu_\nu/\mu_B < 6.6 \times 10^{-11}$. As a comparison, the best measurement of $\sin^2 \theta_W$ at low energy transfer is the atomic parity violation (APV) experiment, 0.238 ± 0.005 (1σ) [37]. From the COHERENT experiment, the value of $\sin^2 \theta_W$ is $0.26^{+0.04}_{-0.03}$ (1σ) [38]. The best limit for μ_ν is $\mu_\nu < 2.9 \times 10^{-11} \mu_B$ measured by GEMMA [39].

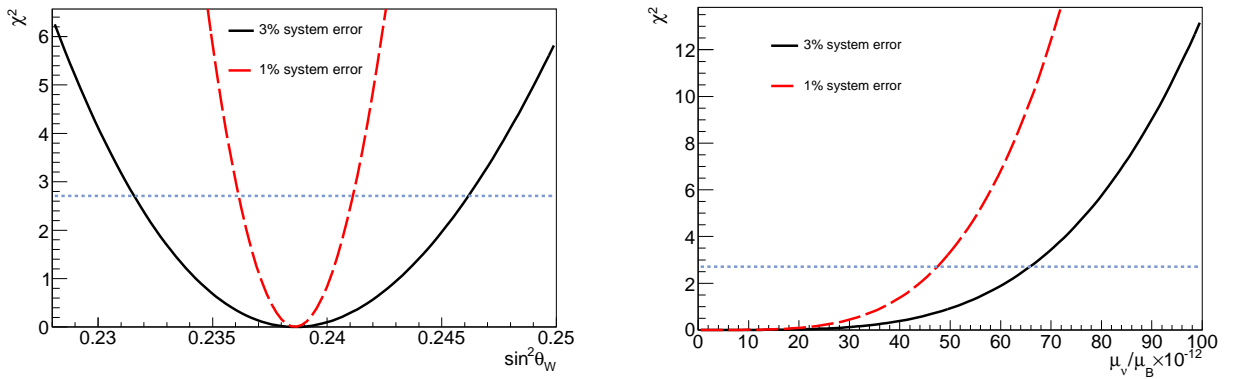


Figure 10: The expected sensitivity of the weak mixing angle $\sin^2 \theta_W$ (left) and of the neutrino magnetic moment μ_ν (right).

It should be noted that above sensitivities are obtained by fixing one parameter and minimizing the other

one. For example, μ_ν is fixed to 0 when studying $\sin^2 \theta_W$. Similarly, $\sin^2 \theta_W$ is fixed at the nominal value when searching for the upper limit of μ_ν . In the future, a joint fitting of $\sin^2 \theta_W$, μ_ν , and Y_{e^-} can be performed based on the large CE ν NS data set.

5 Summary

In this paper, we have put forward a 200 kg dual-phase argon time projection chamber to detect the CE ν NS from the Taishan nuclear reactor. The outer shielding and the active veto are designed. The backgrounds from ambient radioactivity and cosmic-ray muons are simulated. With the help of a single-phase argon detector surrounding the dual-phase TPC, the background level is 153 per day in the energy range of interest. This compares to a CE ν NS signal rate of 955 per day. With the large data set, the expected sensitivities of the weak mixing angle $\sin^2 \theta_W$, the neutrino magnetic moment ν_μ are presented. In addition, a synergy between the reactor antineutrino CE ν NS experiment and the WIMP dark matter experiment is foreseen, not only in the better understanding of the neutrino floor, but also in the understanding of the detector response at keV nuclear recoil energy range.

Acknowledgement

The study is supported by National Key R&D Program of China (2016YFA0400304) and National Natural Science Foundation of China (11975244).

The authors would like to thank Yufeng Li, Yiyu Zhang, and Yi Wang for the helpful discussion.

References

- [1] Daniel Z. Freedman. Coherent effects of a weak neutral current. *Phys. Rev. D*, 9:1389–1392, Mar 1974.
- [2] D. Akimov et al. Observation of Coherent Elastic Neutrino-Nucleus Scattering. *Science*, 357(6356):1123–1126, 2017.
- [3] D. Akimov et al. First Detection of Coherent Elastic Neutrino-Nucleus Scattering on Argon. 3 2020.
- [4] Matteo Cadeddu and Francesca Dordei. Reinterpreting the weak mixing angle from atomic parity violation in view of the Cs neutron rms radius measurement from COHERENT. *Phys. Rev. D*, 99(3):033010, 2019.
- [5] Matteo Cadeddu, Carlo Giunti, Yufeng Li, and Yiyu Zhang. Average CsI neutron density distribution from COHERENT data. *PoS, NuFACT2018:144*, 2018.
- [6] D.K. Papoulias and T.S. Kosmas. COHERENT constraints to conventional and exotic neutrino physics. *Phys. Rev. D*, 97(3):033003, 2018.
- [7] M. Cadeddu, C. Giunti, K.A. Kouzakov, Y.F. Li, A.I. Studenikin, and Y.Y. Zhang. Neutrino Charge Radii from COHERENT Elastic Neutrino-Nucleus Scattering. *Phys. Rev. D*, 98(11):113010, 2018. [Erratum: *Phys.Rev.D* 101, 059902 (2020)].
- [8] E. Aprile et al. Results from a Calibration of XENON100 Using a Source of Dissolved Radon-220. *Phys. Rev. D*, 95(7):072008, 2017.
- [9] Hongguang Zhang et al. Dark matter direct search sensitivity of the PandaX-4T experiment. *Sci. China Phys. Mech. Astron.*, 62(3):31011, 2019.
- [10] C.E. Aalseth et al. DarkSide-20k: A 20 tonne two-phase LAr TPC for direct dark matter detection at LNGS. *Eur. Phys. J. Plus*, 133:131, 2018.
- [11] P. Agnes et al. Low-Mass Dark Matter Search with the DarkSide-50 Experiment. *Phys. Rev. Lett.*, 121(8):081307, 2018.

- [12] E. Aprile et al. Search for Light Dark Matter Interactions Enhanced by the Migdal Effect or Bremsstrahlung in XENON1T. *Phys. Rev. Lett.*, 123(24):241803, 2019.
- [13] D.S. Akerib et al. Improving sensitivity to low-mass dark matter in LUX using a novel electrode background mitigation technique. 11 2020.
- [14] D.K. Papoulias, T.S. Kosmas, and Y. Kuno. Recent probes of standard and non-standard neutrino physics with nuclei. *Front. in Phys.*, 7:191, 2019.
- [15] Jason Newby. Results from coherent, June 2020.
- [16] Alexis Aguilar-Arevalo et al. Exploring low-energy neutrino physics with the Coherent Neutrino Nucleus Interaction Experiment. *Phys. Rev. D*, 100(9):092005, 2019.
- [17] G. Agnolet et al. Background Studies for the MINER Coherent Neutrino Scattering Reactor Experiment. *Nucl. Instrum. Meth. A*, 853:53–60, 2017.
- [18] H. Bonet et al. First constraints on elastic neutrino nucleus scattering in the fully coherent regime from the Conus experiment. 10 2020.
- [19] D. Yu Akimov et al. First ground-level laboratory test of the two-phase xenon emission detector RED-100. *JINST*, 15(02):P02020, 2020.
- [20] Angel Abusleme et al. TAO Conceptual Design Report: A Precision Measurement of the Reactor Antineutrino Spectrum with Sub-percent Energy Resolution. 5 2020.
- [21] P. Agnes et al. Results From the First Use of Low Radioactivity Argon in a Dark Matter Search. *Phys. Rev. D*, 93(8):081101, 2016. [Addendum: Phys.Rev.D 95, 069901 (2017)].
- [22] C.G. Payne, S. Bacca, G. Hagen, W. Jiang, and T. Papenbrock. Coherent elastic neutrino-nucleus scattering on ^{40}Ar from first principles. *Phys. Rev. C*, 100(6):061304, 2019.
- [23] Th.A. Mueller et al. Improved Predictions of Reactor Antineutrino Spectra. *Phys. Rev. C*, 83:054615, 2011.
- [24] Patrick Huber. On the determination of anti-neutrino spectra from nuclear reactors. *Phys. Rev. C*, 84:024617, 2011. [Erratum: Phys.Rev.C 85, 029901 (2012)].
- [25] D.Yu. Akimov et al. Status of the RED-100 experiment. *JINST*, 12(06):C06018, 2017.
- [26] D. Khaitan. Supernova neutrino detection in LZ. *JINST*, 13(02):C02024, 2018.
- [27] G. Carugno, B. Dainese, F. Pietropaolo, and F. Ptohos. Electron lifetime detector for liquid argon. *Nucl. Instrum. Meth. A*, 292:580–584, 1990.
- [28] S. Agostinelli et al. GEANT4: A Simulation toolkit. *Nucl. Instrum. Meth.*, A506:250–303, 2003.
- [29] D. Gastler, E. Kearns, A. Hime, L.C. Stonehill, S. Seibert, J. Klein, W.H. Lippincott, D.N. McKinsey, and J.A. Nikkel. Measurement of scintillation efficiency for nuclear recoils in liquid argon. *Phys. Rev. C*, 85:065811, 2012.
- [30] C. Bungau, B. Camanzi, J. Champer, Y. Chen, D.B. Cline, R. Luscher, J.D. Lewin, P.F. Smith, N.J.T. Smith, and H. Wang. Monte Carlo studies of combined shielding and veto techniques for neutron background reduction in underground dark matter experiments based on liquid noble gas targets. *Astropart. Phys.*, 23:97–115, 2005. [Erratum: Astropart.Phys. 23, 535–535 (2005)].
- [31] P. Agnes et al. First Results from the DarkSide-50 Dark Matter Experiment at Laboratori Nazionali del Gran Sasso. *Phys. Lett. B*, 743:456–466, 2015.

- [32] Feng Peng An et al. Improved Measurement of the Reactor Antineutrino Flux and Spectrum at Daya Bay. *Chin. Phys. C*, 41(1):013002, 2017.
- [33] E. Aprile et al. Light Dark Matter Search with Ionization Signals in XENON1T. *Phys. Rev. Lett.*, 123(25):251801, 2019.
- [34] M. Andriamirado et al. Improved Short-Baseline Neutrino Oscillation Search and Energy Spectrum Measurement with the PROSPECT Experiment at HFIR. 6 2020.
- [35] Helena Almazán Molina et al. First antineutrino energy spectrum from ^{235}U fissions with the STEREO detector at ILL. 10 2020.
- [36] P.A. Zyla et al. Review of Particle Physics. *PTEP*, 2020(8):083C01, 2020.
- [37] M. Cadeddu, F. Dordei, C. Giunti, Y.F. Li, and Y.Y. Zhang. Neutrino, electroweak, and nuclear physics from COHERENT elastic neutrino-nucleus scattering with refined quenching factor. *Phys. Rev. D*, 101(3):033004, 2020.
- [38] M. Cadeddu, F. Dordei, C. Giunti, Y.F. Li, E. Picciau, and Y.Y. Zhang. Physics results from the first COHERENT observation of coherent elastic neutrino-nucleus scattering in argon and their combination with cesium-iodide data. *Phys. Rev. D*, 102(1):015030, 2020.
- [39] A.G. Beda, V.B. Brudanin, V.G. Egorov, D.V. Medvedev, V.S. Pogosov, M.V. Shirchenko, and A.S. Starostin. The results of search for the neutrino magnetic moment in GEMMA experiment. *Adv. High Energy Phys.*, 2012:350150, 2012.